Supporting Information for: Ice residual properties in mixed-phase clouds at the high-alpine Jungfraujoch site

Piotr Kupiszewski[1,2], Marco Zanatta[1,3,4], Stephan Mertes[5], Paul Vochezer[6], Gary Lloyd[7], Johannes Schneider[8], Ludwig Schenk[5], Martin Schnaiter[6], Urs Baltensperger[1], Ernest Weingartner[1,9], Martin Gysel[1]

[1]Laboratory of Atmospheric Chemistry, Paul Scherrer Institute, Villigen, Switzerland.
[2]Now at Department of Meteorology, Stockholm University, Stockholm, Sweden.
[3]Laboratoire de Glaciologie et Géophysique de l'Environnement, Université Grenoble Alpes/CNRS, Grenoble, France.
[4]Now at Alfred Wegener Institute, Helmholtz Centre for Polar and Marine Research, Bremerhaven, Germany.
[5]Leibniz Institute for Tropospheric Research, Leipzig, Germany.
[6]Institute of Meteorology and Climate Research, Karlsruhe Institute of Technology, Karlsruhe, Germany.
[7]Centre for Atmospheric Science, SEAES, University of Manchester, Manchester, UK.
[8]Particle Chemistry Department, Max Planck Institute for Chemistry, Mainz, Germany.
[9]Now at Institute for Aerosol and Sensor Technology, University of Applied Sciences, Windisch, Switzerland.

S1: Potential for scavenging of interstitial aerosol particles by ice crystals

An ice crystal at the Jungfraujoch will grow to $20\,\mu\mathrm{m}$ size within approximately $20\,\mathrm{s}$, assuming an environment saturated with respect to water and a mass accommodation coefficient of 1 (calculated based on the mass transfer equation following *Seinfeld and Pandis* [2006]). When analyzing the ice residuals extracted from these ice crystals, the question arises whether the ice crystals could have scavenged interstitial aerosol particles. In order to assess the likelihood of this taking place during the time it takes for the ice crystal to grow to the size range sampled by the Ice-CVI we perform a simple calculation of the collision rate of a particle with a diameter of $D_{p1} = 20\,\mu\mathrm{m}$ (i.e. the ice crystal) with aerosol particles with a diameter $D_{p2} = 200\,\mathrm{nm}$. We assume a number concentration of $N_2 = 100\,\mathrm{cm}^{-3}$ for the aerosol particles. The collision rate J_{col}, which in this case is the number of aerosol particles which collide with a single ice crystal per second, can be calculated as follows (see e.g. *Seinfeld and Pandis* [2006]):

$$J_{\mathrm{col}} = 2\pi(D_{p1} + D_{p2})(D_1 + D_2)N_2 \tag{1}$$

where D is the Brownian diffusion coefficient.

The collision rate obtained is $1.47 \cdot 10^{-6}\,\mathrm{s}^{-1}$. If the aerosol particles are assumed to have a diameter of $100\,\mathrm{nm}$ instead of $200\,\mathrm{nm}$ the collision rate is $2.9 \cdot 10^{-6}\,\mathrm{s}^{-1}$. Assuming a sticking probability of 1, the collision rate is equivalent to the coagulation rate. An ice crystal will thus undergo a collision and coagulation event with an interstitial particle approximately every 190 hrs and 96 hrs assuming $200\,\mathrm{nm}$ and $100\,\mathrm{nm}$ intersitial particles, respectively. The very low collision rates thus indicate that it is very unlikely that ice crystals will scavenge aerosol particles in the time it takes them to grow to $20\,\mu\mathrm{m}$ and the small ice crystals sampled through the Ice-CVI are thus very unlikely to contain scavenged material.

S2: Ice-CVI background (out-of-cloud) size distributions

Background out-of-cloud size distributions were measured downstream of the Ice-CVI with the aim of assessing whether the contribution of potential sampling artifacts, such as transmission of interstitial aerosol particles, wind-blown snow, or memory-effects of the long Ice-CVI inlet, could affect the measured in-cloud ice residual number size distributions. The CVI counterflow was on during these periods, so these events show the typical background measured downstream of the Ice-CVI when sampling out-of-cloud in CVI mode. In Fig. S1 the average size distributions for nine background events are presented. In order to get an idea of the magnitude of background measurements relative to in-cloud ice residual measurements these size distributions can be compared with the in-cloud size distributions presented in Fig. 5 of the paper.

The comparison shows that background size distributions are considerably lower than in-cloud ice residual size distributions. This is perhaps seen even more clearly in Fig. S2, where we present the medians of the event average size distributions for both in-cloud (continuous lines) and out-of-cloud measurements (dotted lines), as well as the ratios of in-cloud to out-of-cloud measurements (dashed lines). The ratios are between approximately 10 and 20, confirming that background counts are a very minor fraction of the measured in-cloud size distributions

Corresponding author: Martin Gysel, martin.gysel@psi.ch

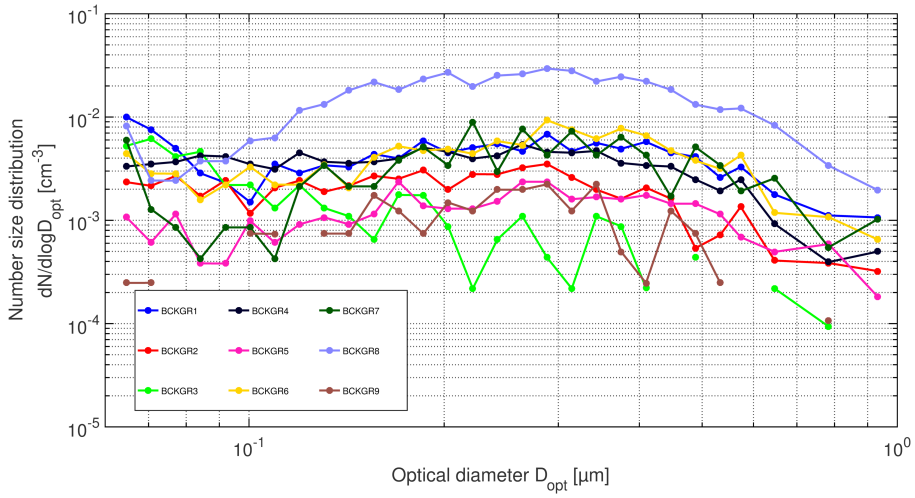

Figure S1. Background particle number size distributions measured downstream of the Ice-CVI during nine out-of-cloud events.

and, under the assumption that the background is identical for out-of-cloud and in-cloud conditions, potential sampling artifacts do not have a significant effect on the presented ice residual number size distributions.

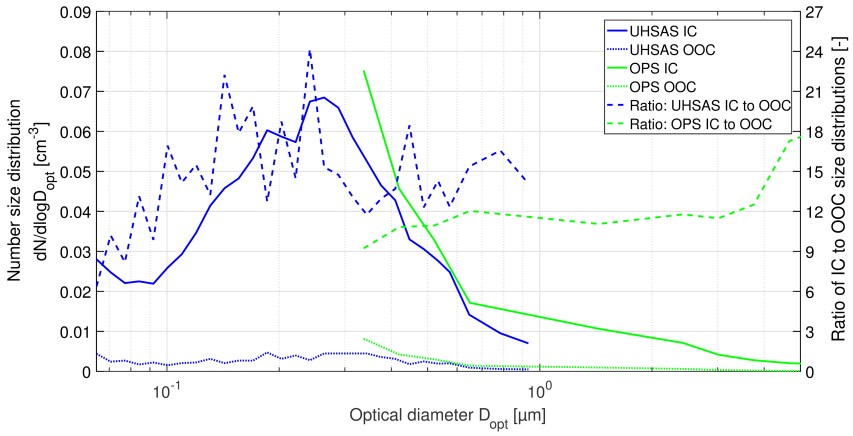

Figure S2. In-cloud (IC) and out-of-cloud (OOC; background) particle number size distributions measured downstream of the Ice-CVI, and the ratio of the IC to OOC number size distributions. The size distributions shown are the medians of the CLACE 2013 cloud event averages (in the case of IC size distributions) and the medians of the CLACE 2013 background event averages (in the case of OOC size distributions).

Background out-of-cloud size distributions were also compared with the ambient (total inlet; TI) size distributions in order to estimate the rejection efficiency of aerosol particles by the Ice-CVI as a function of particle size. The ratio of background (out-of-cloud) Ice-CVI size distributions to ambient (TI) size distributions (see Fig. S3) shows a strong dependency on size, with larger particles preferentially passing through the Ice-CVI. The preferential transmission of larger particles through the Ice-CVI may be due to imperfect filtering of thin cloud events when selecting out-of-cloud data, sampling of wind-blown snow under clear-sky conditions, or possibly a memory effect resulting from deposition and subsequent release of ice crystals in the long sequence of modules which form the Ice-CVI. If the Ice-CVI occasionally samples ice crystals when assumed to be out of cloud, or occasionally releases ice crystals deposited within the inlet during in-cloud sampling, the ice residuals released will skew the measured background size distributions to larger sizes. This hypothesis is supported by the fact that the Ice-CVI out-of-cloud size distributions are similar in shape to the ice residual size distributions measured in cloud. It is important to highlight that although the background Ice-CVI concentrations may be subject to some sampling artifacts, the in-cloud size distributions are an order of magnitude higher. Assuming that the

background does not differ for in-cloud and out-of-cloud conditions, it is can thus be concluded that the particles measured downstream of the Ice-CVI in-cloud are residuals of cloud particles.

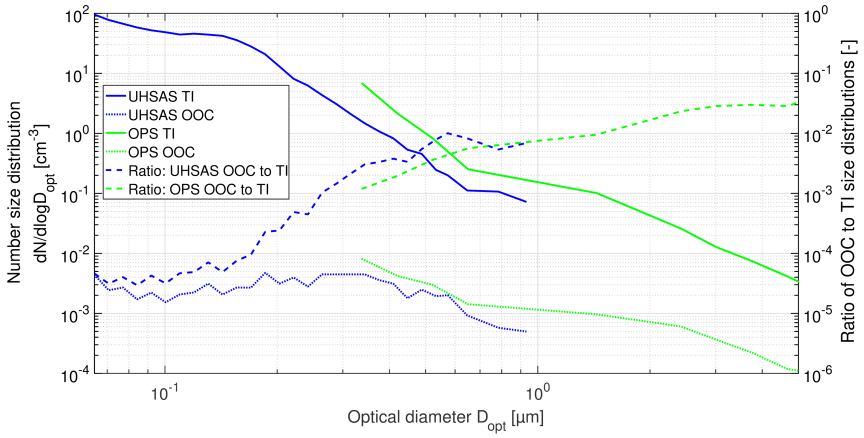

Figure S3. Ambient (total inlet; TI) and out-of-cloud (OOC; background) particle number size distributions measured downstream of the Ice-CVI, and the ratio of the OOC to TI number size distributions. The size distributions shown are the medians of the CLACE 2013 TI event averages (in the case of TI size distributions) and the medians of the CLACE 2013 background event averages (in the case of OOC size distributions).

To ensure that the concentrations of cloud particle residuals measured are not governed by potential breakthrough of supercooled liquid droplets through the Ice-CVI we compare the concentrations measured by the Ice-CVI CPC during cloud periods with ice crystals (ice-containing clouds) and without ice crystals (liquid clouds). Ice crystal number concentrations are derived from the Two Dimensional-Stereoscopic (2D-S) probe, which provides ice crystal concentrations in the size range of approximately $60 - 1280\,\mu\mathrm{m}$. As the arbitrary threshold for ice-containing clouds we take an ice crystal number concentration of $10\,\mathrm{L}^{-1}$. It should be noted that the ice crystal number concentration obtained from the 2D-S is for a different size range to the ice crystal size range targeted by the Ice-CVI ($5 - 20\,\mu\mathrm{m}$). Therefore, the ice crystal number concentration from the 2D-S can only be used as a marker for ice occurence, and cannot be compared directly with the particle number concentrations measured downstream of the Ice-CVI. Furthermore, as it is not clear how closely concentrations of smaller and larger ice crystals are related, the analysis presented here is subject to considerable uncertainties. The statistics for concentrations of particles measured downstream of the Ice-CVI in ice-containing and in liquid clouds (calculated based on one minute averages), derived from the 15 cloud events analyzed during CLACE 2013 are shown in Table. S1. The comparison shows an order of magnitude higher concentrations in ice-containing clouds, as compared to liquid clouds. This is a clear indication that potential transmission of liquid droplets through the Ice-CVI does not have any significant contribution on the ice residual concentrations measured.

Table S1. Ice-CVI number concentrations [L^{-1}] in ice-containing clouds and in liquid clouds, as measured by a condensation particle counter (CPC).

	Ice-containing clouds	**Liquid clouds**
CPC mean	1202	196
CPC median	368	27
CPC lower quartile	104	9
CPC upper quartile	1212	74

S3: Scanning Mobility Particle Sizers

Both SMPS systems were custom-built at PSI and their operation was verified in a study by *Wiedensohler et al.* [2012]. The SMPS behind the total inlet (SMPS TI) consisted of a differential mobility analyser (DMA; model 3071, TSI, USA) and a condensation particle counter (CPC; model 3775, TSI, USA). The other system behind the Ice-CVI (SMPS Ice-CVI) consisted of a TSI long type DMA (custom-built at PSI) and a CPC model 3022A (TSI, USA). Both DMAs were operated with a sheath air flow rate of $3\,\mathrm{L\,min}^{-1}$ and a sample air flow rate of $0.3\,\mathrm{L\,min}^{-1}$. As the tubing connecting the SMPS Ice-CVI to the Ice-CVI was of considerable length ($\sim 2.5\,\mathrm{m}$),

the SMPS Ice-CVI size distributions were corrected to account for tubing losses (10-21 % for particles with D_{mob} in the 16-35 nm range and $< 10\,\%$ for particles with $D_{\mathrm{mob}} > 35\,\mathrm{nm}$) using the Particle Loss Calculator [*von der Weiden et al.*, 2009]. A particle density of $2\,\mathrm{g\,cm^{-3}}$ was used for the corrections, as assumed for IR density by *Cozic et al.* [2008].

S4: Optical Particle Size Spectrometers (UHSAS, Grimm OPSS, WIBS3 and TSI OPS)

Size distributions measured by the Grimm 1.129 optical particle size spectrometer (OPSS), which was set up a considerable distance from the Ice-CVI and total inlet (1.26 m and 2.61 m, respectively) were corrected for tubing losses following the same procedure as used for the SMPS size distribution corrections. The losses for the Ice-CVI were $< 10\,\%$ and 10-64 % for particles with $D_{\mathrm{opt}} < 1.8\,\mu\mathrm{m}$ and particles with D_{opt} in the $1.8 - 5\,\mu\mathrm{m}$ range, respectively. For the total inlet the losses were $< 10\,\%$ and 10-100 % for particles with $D_{\mathrm{opt}} < 1.2\,\mu\mathrm{m}$ and particles with D_{opt} in the $1.2 - 5\,\mu\mathrm{m}$ range, respectively. Due to the high losses in the tubing between the total inlet and the Grimm 1.129, the Grimm 1.129 size distributions for the total inlet are shown only for particles with diameters up to $3.5\,\mu\mathrm{m}$ (at this diameter losses reached 65 %). Number size distributions with respect to optical particle diameter were also obtained from the WIBS3 [*Foot et al.*, 2008; *Gabey et al.*, 2010; *Kaye et al.*, 2005]. The reduction in counting efficiency of the WIBS3 towards its lower detection limit measured by *Gabey et al.* [2011] was used to correct the raw WIBS3 size distributions.

All the OPSSs used were calibrated using polystyrene latex spheres with a refractive index (RI) of 1.59. As the RI of the aerosol is not known we are not able to correct the measured optical sizes for the true RI and thus there is some systematic error in the size distributions shown. In order to get an approximate idea of the magnitude of the error in the submicrometer size range, we have calculated the change in optical diameter for the UHSAS instrument assuming an RI of 1.5. The relative change in optical diameter assuming an RI of 1.59 versus an RI of 1.5 is $5 - 19\,\%$, with higher values towards the upper range of the UHSAS. In the supermicrometer size range additional uncertainties in the derived size from the ambiguity in sizing due to the non-monotonic relationship between particle size and the intensity of scattered light, as well as from the influence of the unaccounted for imaginary part of the RI become increasingly important.

S5: Ice-CVI performance: comparison of ice residual and small ice crystal number concentrations

Ice residual (IR) and small ice crystal number concentrations measured during the case study period showed reasonable agreement with a correlation coefficient r^2 of 0.6. Perfect agreement between the two instruments cannot be expected, as the optical diameter size range measured by the SID-3 is not directly comparable with the aerodynamic diameter size range sampled by the Ice-CVI. In addition, the cutoff curves, which define the endpoints of these ranges, are not sharp. It is expected that they experience different steepness which also affects the encountered concentrations. Furthermore, for the SID-3 number concentration measurement of ice crystals, the size range used should be somewhat broader than the $5 - 20\,\mu\mathrm{m}$ range, as the SID-3 calibration is conducted using spherical liquid droplets which have different optical properties as compared to ice crystals. In the angular detection range of the SID-3 trigger detector ($50\,^\circ \pm 9\,^\circ$) ice particles have a higher scattering cross section than liquid droplets [*Järvinen et al.*, 2016], which results in oversizing of irregular (complex) ice particles, such as the frozen droplets occurring in mixed-phase clouds. This in turn means that the upper end of the SID-3 size range should be extended to somewhat higher values than $20\,\mu\mathrm{m}$. On the other hand, more pristine hexagonal ice particles are tendentially undersized as their sizing is strongly dependent on the particle orientation and it is highly unlikely that the particle comes in the right orientation to get the gross of scattered intensity by the angularly confined trigger detector (pristine particles have a highly non-uniform spatial scattering behavior with the majority of the intensity located only in a few spots [*Schnaiter et al.*, 2016]). Consequently, the lower edge of the size range should be extended to somewhat smaller sizes than $5\,\mu\mathrm{m}$. The size ranges of ice crystals sampled by the Ice-CVI and measured by the SID-3 are thus not exactly the same, with the SID-3 size range, calibrated based on spherical liquid droplet measurements, narrower than it should be for measuring ice particle concentration in the $5 - 20\,\mu\mathrm{m}$. However, the differences are very difficult to quantify and thus we have used the $5 - 20\,\mu\mathrm{m}$ size range in order to avoid arbitrarily selecting a broader size range. The difference in the diameter measurements is likely to contribute significantly to the discrepancies between the CPC IR and the SID-3 ice crystal concentrations. Unfortunately, as the Ice-CVI and SID-3 use different physical principles for extracting/measuring ice crystals, a better comparison is very difficult. Moreover, the Ice-CVI and SID-3 were mounted some meters apart, on separate terraces. As such they were exposed to different wind, and thus sampling conditions; this difference was further magnified by the fact that the SID-3 automatically adjusts to face into the wind, while the Ice-CVI samples using an omni-directional inlet. As there are buildings and structures

between the SID-3 and the Ice-CVI, it is likely that their sampling efficiency is affected differently by different wind conditions. Nevertheless, based on the case study we qualitatively confirm that the Ice-CVI is selectively sampling and extracting small ice crystals.

S6: Assessment of inter-comparability of optical particle size spectrometer measurements

The differences in the size distributions measured by the optical particle size spectrometers at larger sizes are systematically biased, with the instruments in order of highest to lowest counts at a given number concentrations generally ordered as follows: TSI OPS, Grimm 2, Grimm 1 and WIBS3. While we have corrected the measurements for tubing losses and size dependence of counting efficiency, as described in Sections S1 and S2, the corrections are insufficient to account for all inconsistencies. Differences in calibration and sizing methods of the instruments may be one of the principal reasons for the disagreement; such differences will lead to the size distributions being shifted in the horizontal with respect to one another. A further reason for the discrepancies are sizing ambiguities arising from Mie oscillations in the size dependence of the scattering cross section of a given particle type, the importance of which depends on the size parameter and the distinct angular detection specifications of the instruments. The pronounced local maximum at an optical diameter of $\sim 2.5\,\mu\mathrm{m}$ in all size distributions measured by the Grimm OPSSs is an example of such sizing artifacts.

S7: Ice residual size distribution measurements

Table S2. Instrumentation measuring ice residuals during CLACE 2013 cloud events.

Cloud event	CPC	SMPS Ice-CVI	UHSAS	SP2	WIBS	Grimm 1	TSI OPS
1	✓	✓	✓	✗	✓	✓	✓
2	✓	✗	✓	✗	✗	✓	✓
3	✓	✓	✗	✗	✗	✓	✓
4	✓	✓	✓	✗	✓	✗	✓
5	✓	✗	✓	✗	✓	✗	✓
8	✓	✗	✓	✗	✓	✗	✓
9	✓	✓	✓	✓	✓	✗	✓
10	✓	✓	✓	✓	✓	✗	✓
11	✓	✗	✓	✗	✗	✓	✓
12	✓	✗	✓	✗	✓	✓	✓
13	✓	✓	✓	✓	✓	✗	✓
14	✓	✗	✓	✓	✓	✗	✓
17	✓	✗	✗	✗	✗	✗	✓
18	✓	✓	✓	✓	✗	✓	✓
21	✓	✗	✗	✗	✗	✗	✓

S8: Potential dust interference in eBC mass concentration

The potential interference from mineral dust absorption in the determination of eBC mass in the IR was corrected for by *Cozic et al.* [2008] in the following manner: the ice residual size distribution based on SMPS and Grimm measurements (size range of $17\,\mathrm{nm}$ to $20\,\mu\mathrm{m}$) was converted into a maximum mineral dust mass concentration, assuming that the whole volume corresponds to mineral dust and using a density of $2.5\,\mathrm{g\,cm^{-3}}$. The corresponding maximal contribution of mineral dust to the absorption coefficient was subsequently estimated using a MAC ($\lambda = 565\,\mathrm{nm}$) of $0.04\,\mathrm{m^2\,g^{-1}}$ for mineral dust, following *Cozic et al.* [2008]. The upper limit of the mineral dust (relative) interference in the eBC mass concentration was then obtained from the ratio of estimated absorption coefficient of mineral dust to the total absorption coefficient measured by the PSAP, and was found to be 15 % on average. However, the dust interference may have been underestimated by *Cozic et al.* [2008] for two main reasons: Firstly, as shown in this work, there are large uncertainties in the size distributions derived by OPSS instruments at larger sizes, with the Grimm size distributions generally considerably lower than the TSI OPS size distributions (see Sect. 3.3 of the paper). Undercounting of the Grimm OPSS and/or losses of large particles in the tubing between the Ice-CVI and the Grimm OPSS would have resulted in a low-bias in the assumed mineral dust mass concentration and, therefore, an underestimation of the mineral dust inference.

Secondly, the MAC of dust may have been underestimated by *Cozic et al.* [2008]. We assess the likelihood of a dust interference issue with the data set available in this study, by separately comparing simultaneous PSAP and SP2 measurements with each other for both total and ice residual samples. The PSAP absorption measurements were corrected following *Bond et al.* [1999], whereas the term including the scattering coefficient was, for lack of appropriate data, ignored as also done in *Cozic et al.* [2008]. Dividing the PSAP derived absorption coefficient, which includes potential dust interference, by the SP2 derived rBC mass concentration, which does not suffer from dust interference, provides an apparent MAC value of rBC. The respective values for the total and ice residual samples were $14\,\mathrm{m^2\,g^{-1}}$ and $1000\,\mathrm{m^2\,g^{-1}}$ (at $\lambda = 565\,\mathrm{nm}$). The apparent MAC for the total aerosol

is physically reasonable and, within uncertainty, in agreement with previous measurements at the Jungfraujoch site [*Liu et al.*, 2010]. The apparent MAC for the ice residuals is two orders of magnitude larger than physically possible. This gives clear evidence that the absorption is dominated by dust rather than BC, which results in a massive high bias in the PSAP-derived eBC mass concentrations. A low bias in the SP2 derived rBC mass concentration, if a substantial fraction of BC mass was above the upper detection limit of the SP2 for BC cores, may also contribute to the difference in the results presented in this paper and those obtained by *Cozic et al.* [2008]. Indeed, the rBC core size distribution in the ice residuals is distinctly shifted towards larger sizes. However, if the dominant fraction of rBC mass were above the upper size limit of the SP2, this would also imply that most rBC mass is associated with very few large BC cores, thus making BC mass invalid as a predictor for the number of BC-containing particles.

References

Bond, T. C., T. L. Anderson, and D. Campbell (1999), Calibration and intercomparison of filter-based measurements of visible light absorption by aerosols, *Aerosol Sci. Technol.*, *30*(6), 582–600, doi:10.1080/027868299304435.

Cozic, J., S. Mertes, B. Verheggen, D. J. Cziczo, S. J. Gallavardin, S. Walter, U. Baltensperger, and E. Weingartner (2008), Black carbon enrichment in atmospheric ice particle residuals observed in lower tropospheric mixed phase clouds, *J. Geophys. Res. Atmos.*, *113*(D15), doi:10.1029/2007JD009266.

Foot, V. E., P. H. Kaye, W. R. Stanley, S. J. Barrington, M. Gallagher, and A. Gabey (2008), Low-cost real-time multiparameter bio-aerosol sensors, *Proc. SPIE*, *7116*, 71,160I–71,160I–12, doi:10.1117/12.800226.

Gabey, A. M., M. W. Gallagher, J. Whitehead, J. R. Dorsey, P. H. Kaye, and W. R. Stanley (2010), Measurements and comparison of primary biological aerosol above and below a tropical forest canopy using a dual channel fluorescence spectrometer, *Atmos. Chem. Phys.*, *10*(10), 4453–4466, doi:10.5194/acp-10-4453-2010.

Gabey, A. M., W. R. Stanley, M. W. Gallagher, and P. H. Kaye (2011), The fluorescence properties of aerosol larger than $0.8\mu\mathrm{m}$ in urban and tropical rainforest locations, *Atmos. Chem. Phys.*, *11*(11), 5491–5504, doi:10.5194/acp-11-5491-2011.

Järvinen, E., M. Schnaiter, G. Mioche, O. Jourdan, V. N. Shcherbakov, A. Costa, A. Afchine, M. Krämer, F. Heidelberg, T. Jurkat, C. Voigt, H. Schlager, L. Nichman, M. Gallagher, E. Hirst, C. Schmitt, A. Bansemer, A. Heymsfield, P. Lawson, U. Tricoli, K. Pfeilsticker, P. Vochezer, O. Möhler, and T. Leisner (2016), Quasi-spherical ice in convective clouds, *J. Atmos. Sci.*, doi:10.1175/JAS-D-15-0365.1.

Kaye, P., W. R. Stanley, E. Hirst, E. V. Foot, K. L. Baxter, and S. J. Barrington (2005), Single particle multichannel bio-aerosol fluorescence sensor, *Opt. Express*, *13*(10), 3583–3593, doi:10.1364/OPEX.13.003583.

Liu, D., M. Flynn, M. Gysel, A. Targino, I. Crawford, K. Bower, T. Choularton, Z. Jurányi, M. Steinbacher, C. Hüglin, J. Curtius, M. Kampus, A. Petzold, E. Weingartner, U. Baltensperger, and H. Coe (2010), Single particle characterization of black carbon aerosols at a tropospheric alpine site in Switzerland, *Atmos. Chem. Phys.*, *10*(15), 7389–7407, doi:10.5194/acp-10-7389-2010.

Schnaiter, M., E. Järvinen, P. Vochezer, A. Abdelmonem, R. Wagner, O. Jourdan, G. Mioche, V. N. Shcherbakov, C. G. Schmitt, U. Tricoli, Z. Ulanowski, and A. J. Heymsfield (2016), Cloud chamber experiments on the origin of ice crystal complexity in cirrus clouds, *Atmos. Chem. Phys.*, *16*(8), 5091–5110, doi:10.5194/acp-16-5091-2016.

Seinfeld, J. H., and S. N. Pandis (2006), *Atmospheric Chemistry and Physics: From Air Pollution to Climate Change, 2nd Edition*, John Wiley & Sons, Inc., Hoboken, New Jersey.

von der Weiden, S.-L., F. Drewnick, and S. Borrmann (2009), Particle Loss Calculator – a new software tool for the assessment of the performance of aerosol inlet systems, *Atmos. Meas. Tech.*, *2*(2), 479–494, doi:10.5194/amt-2-479-2009.

Wiedensohler, A., W. Birmili, A. Nowak, A. Sonntag, K. Weinhold, M. Merkel, B. Wehner, T. Tuch, S. Pfeifer, M. Fiebig, A. M. Fjäraa, E. Asmi, K. Sellegri, R. Depuy, H. Venzac, P. Villani, P. Laj, P. Aalto, J. A. Ogren, E. Swietlicki, P. Williams, P. Roldin, P. Quincey, C. Hüglin, R. Fierz-Schmidhauser, M. Gysel, E. Weingartner, F. Riccobono, S. Santos, C. Grüning, K. Faloon, D. Beddows, R. Harrison, C. Monahan, S. G. Jennings, C. D. O'Dowd, A. Marinoni, H.-G. Horn, L. Keck, J. Jiang, J. Scheckman, P. H. McMurry, Z. Deng, C. S. Zhao, M. Moerman, B. Henzing, G. de Leeuw, G. Löschau, and S. Bastian (2012), Mobility particle size spectrometers: harmonization of technical standards and data structure to facilitate high quality long-term observations of atmospheric particle number size distributions, *Atmos. Meas. Tech.*, *5*(3), 657–685, doi:10.5194/amt-5-657-2012.